THE JOURNAL OF PHYSICAL CHEMISTRY C
A JOURNAL OF THE AMERICAN CHEMICAL SOCIETY

pubs.acs.org/JPCC

Article

Anion Substitution Effects on the Structural, Electronic, and Optical Properties of Inorganic $CsPb(I_{1-x}Br_x)_3$ and $CsPb(Br_{1-x}Cl_x)_3$ Perovskites: Theoretical and Experimental Approaches

Hamid M. Ghaithan,* Saif M. H. Qaid,* Zeyad A. Alahmed,* Mahmoud Hezam, Andreas Lyras, Mabrook Amer, and Abdullah S. Aldwayyan*

Cite This: J. Phys. Chem. C 2021, 125, 886–897

Read Online

ACCESS | Metrics & More | Article Recommendations | Supporting Information

ABSTRACT: Several inorganic perovskites of iodine, bromine, and chlorine halides have emerged as candidates for various optoelectronic devices. High-quality $CsPb(I_{1-x}Br_x)_3$ and $CsPb(Br_{1-x}Cl_x)_3$ (x = 0.00, 0.25, 0.50, 0.75, and 1.00) inorganic perovskite thin films were prepared in this study using a thermal evaporation system. Experiments and first-principles calculations were conducted to elucidate the structural, electronic, and optical properties of the prepared films at room temperature. The thin-film perovskite band gap was tuned from 1.85 to 3.13 eV by replacing I^- with Br^- and then Cl^-. Dominant excitonic effects on the onset of optical absorption led us to explicitly account for enhancing absorption through the Sommerfield factor, enabling us to extract the electronic band gap and the exciton binding energy correctly. We correlated our experimental results with the theory of first principles and gained insight into the lattice parameters, electronic structure, excitonic binding energy (E_b), dielectric constant (ε), and reduced effective mass (μ) of the carriers. With increasing concentration (x) of Br and Cl, the E_b increased from 39.44 meV for pure $CsPbI_3$ to 63.04 and 96.73 meV for pure $CsPbBr_3$ and $CsPbCl_3$, respectively, because of a decrease in the dielectric constant and the almost constant value of μ at ∼0.051 m_e. The Urbach energy (E_U) was calculated and found to fluctuate between 28 and 77 meV.

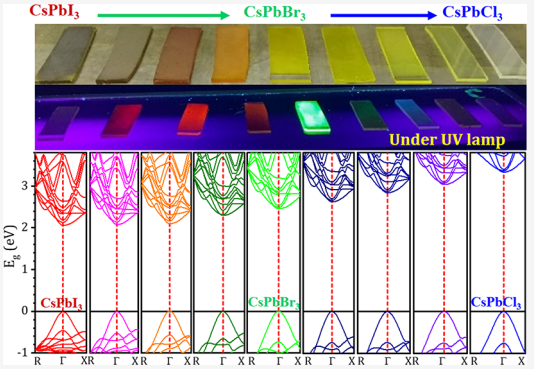

1. INTRODUCTION

Organic–inorganic lead halide perovskites have emerged as essential materials in various optoelectronic devices, including solar cells,[1−8] perovskite light-emitting diodes, and lasers.[9−28] The compatibility of perovskite thin films with low-temperature deposition techniques makes them low-cost materials that provide high carrier mobility when cast as polycrystalline films.[29] High-quality perovskite polycrystalline thin films or single crystals can be easily synthesized using several methods.[30−32] Vapor-based techniques are a mature technology widely used in the coating and semiconductor industries.[33,34] Vacuum deposition methods offer additional benefits for the deposition of perovskite thin films, such as intrinsically pure sublimated materials, film thickness control, and a low substratum manufacturing temperature.[33,34] In addition, compared with solution processes, vacuum deposition methods offer advantages, such as avoiding the use of toxic solvents and the potential for large-scale production.[33−37] Uniform and compact perovskite thin films have enabled researchers to elucidate their electronic properties so that their incorporation into optoelectronic devices is feasible. However, in the case of all-inorganic $CsPb(I_{1-x}Br_x)_3$ and $CsPb(Br_{1-x}Cl_x)_3$ perovskites, few findings address in great detail the role of excitonic states in these materials.[38] The successful development of high-performance optoelectronic devices necessitates a full understanding of the structural, electronic, and optical properties of the wider range of inorganic perovskites.

In the present paper, we describe our preparation of high-quality, uniform, and compact all-inorganic $CsPb(I_{1-x}Br_x)_3$ and $CsPb(Br_{1-x}Cl_x)_3$ perovskite thin films using the thermal evaporation method. The structural, morphological, electronic, and optical properties for a wide range of compositions with band gaps (E_g) ranging from 1.85 to 3.13 eV are discussed. The experimentally observed band gaps and exciton binding energies (E_b) were compared with values obtained from the most accurate method in density functional theory (DFT) calculations: the modified Becke–Johnson potential with the generalized gradient approximation (mBJ-GGA). The DFT investigations of mixed $CsPb(I_{1-x}Br_x)_3$ and $CsPb(Br_{1-x}Cl_x)_3$

Received: September 2, 2020
Revised: December 7, 2020
Published: January 6, 2021

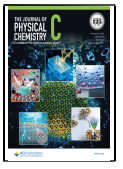

https://dx.doi.org/10.1021/acs.jpcc.0c07983
J. Phys. Chem. C 2021, 125, 886–897

perovskite compositions offer useful insights into their electronic structure as a composition function to identify the particular material. Our work provides an understanding of these optoelectronic materials and also provides a guideline for the design of new materials with desired properties in a similar family of halide perovskite materials.

2. EXPERIMENTAL SECTION

2.1. Chemicals. Lead(II) bromide ($PbBr_2$, 99.999% trace metals basis), lead(II) iodide (PbI_2, 99.999% trace metals basis), lead(II) chloride ($PbCl_2$, 99.999% trace metals basis), cesium iodide (CsI, 99.999% trace metals basis), cesium bromide (CsBr, 99.999% trace metals basis), and cesium chloride (CsCl, 99.999% trace metals basis) were purchased from Sigma–Aldrich. All chemicals were used without further purification.

2.2. Preparation of $CsPb(I_{1-x}Br_x)_3$ and $CsPb(Br_{1-x}Cl_x)_3$ Thin Films. Glass substrates were cleaned using detergent in an ultrasonication bath, followed by ultrasonication in deionized water, acetone, and ethanol for approximately 30 min each. For a pure $CsPbBr_3$ thin film, a 1:1 molar ratio of CsBr and $PbBr_2$ were loaded into a single boat inside the vacuum chamber of a thermal evaporation system. The glass substrates were placed in a holder facing the sources. After the pressure of the evaporator chamber was reduced to 10^{-4} mbar to allow evaporation and transfer of the material to the substrate with only few collisions with ambient gas molecules, the two precursors were evaporated together by increasing the current applied to the tungsten boat (Figure 1). For pure $CsPbI_3$ and $CsPbCl_3$ thin films, CsI and CsCl were used with PbI_2 and $PbCl_2$, respectively.

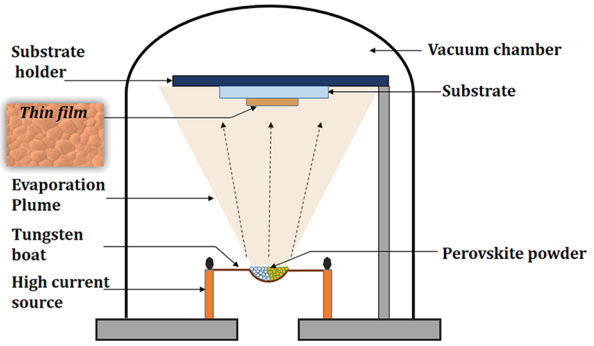

Figure 1. Schematic of the thermal evaporation system.

We mixed the perovskites in appropriate $CsPbBr_3/CsPbI_3$ and $CsPbCl_3/CsPbBr_3$ molar ratios to tune the structural and optical properties of $CsPb(I_{1-x}Br_x)_3$ and $CsPb(Br_{1-x}Cl_x)_3$ perovskite thin films with x = 0.00, 0.25, 0.50, 0.75, and 1.00. Figure 2a–i shows images of two rows of the prepared thin films under ordinary room light (upper row) and under a UV lamp (lower row).

2.3. Perovskite Thin Film Characterization. The absorption and photoluminescence (PL) spectra of the perovskite thin films were recorded using a UV–vis spectrophotometer (JASCO V-670) and a PL spectrometer (Hitachi F-4600), respectively. The transmittance (T) and reflectance (R) were obtained using a Cary 5000 UV–vis–NIR spectrophotometer over the wavelength range of 200–1000 nm. The film thickness was measured using a 3D Surface Profilometer (Veeco Dektak 150). X-ray diffraction (XRD) measurements were performed using a Rigaku Miniflex 600 X-ray diffractometer equipped with a Cu Kα radiation source (40 kV, 15 mA). The morphology was investigated by scanning electron microscopy (SEM) (JEOL-7600F, JEOL, Japan).

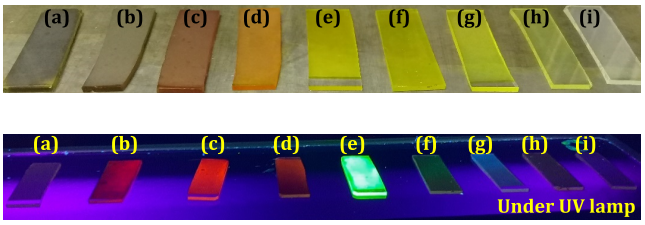

Figure 2. Images of perovskite thin films prepared using a thermal evaporation system under ordinary room light (upper)and under illumination by a UV lamp (lower): (a) $CsPbI_3$, (b) $CsPb(I_{0.75}Br_{0.25})_3$, (c) $CsPb(I_{0.50}Br_{0.50})_3$, (d) $CsPb(I_{0.25}Br_{0.75})_3$, (e) $CsPbBr_3$, (f) $CsPb(Br_{0.75}Cl_{0.25})_3$, (g) $CsPb(Br_{0.50}Cl_{0.50})_3$, (h) $CsPb(Br_{0.25}Cl_{0.75})_3$, and (i) $CsPbCl_3$.

3. COMPUTATIONAL METHOD

Equilibrium geometric structures and electronic and optical properties of the 1 × 1 × 2 $CsPb(I_{1-x}Br_x)_3$ and $CsPb(Br_{1-x}Cl_x)_3$ supercells (SCs) were calculated with DFT using the WIEN2k code.[39,40] The exchange–correlation potential schemes for the structural properties were calculated using the Perdew–Burke–Ernzerhof GGA modified for solids (PBEsol-GGA).[41] The $CsPb(I_{1-x}Br_x)_3$ and $CsPb(Br_{1-x}Cl_x)_3$ structures were obtained via the construction of a 1 × 1 × 2 SC, where the orthorhombic unit cell of the binary perovskites had a space group of *Pnma*. The crystal structures were visualized using the Visualization for Electronic and Structural Analysis (VESTA) program.[42]

The electronic properties were evaluated using the mBJ-GGA potentials with consideration of the spin-orbit coupling (SOC) interaction.[43–45] The calculated band gap with SOC was corrected to match the experimental values using the alloy formula.[46–48] The basis function was expanded to $R_{mt} \times K_{max}$ = 9, where R_{mt} represents the smallest muffin-tin radius of all the microscopic spheres in the unit cell, and K_{max} represents the plane-wave cutoff. The wave functions in the muffin-tin spheres were expanded to l_{max} = 10. For all of the mixed structures, a 100 k-point mesh was centered at the Γ-point in the Brillouin zone, where the total energy was converged until it was $<10^{-4}$ Ry. The theoretical estimates of dielectric constants and reduced effective mass μ_r were used to determine the excitonic binding energy (E_b) for these materials.

4. RESULTS AND DISCUSSION

At room temperature, $CsPbI_3$, $CsPbBr_3$, and $CsPbCl_3$ have an orthorhombic structure with space group *Pnma* (no. 62),[49–57] where the unit cell contains one formula unit. Figure S1 in the Supporting Information shows the crystal structure of a 1 × 1 × 2 SC of $CsPb(I_{1-x}Br_x)_3$ and $CsPb(Br_{1-x}Cl_x)_3$ formed from orthorhombic-structured $CsPbI_3$, $CsPbBr_3$, and $CsPbCl_3$. XRD analysis was performed at room temperature to evaluate the crystallinity of the samples. Figure 3 a,b shows the experimental and theoretical XRD patterns. The theoretical XRD patterns were calculated using VESTA software.[42] The diffraction peaks of $CsPbI_3$ gradually shifted toward those of $CsPbBr_3$ and $CsPbCl_3$ as x was increased from 0.00 to 1.00. In Figure 3a, the XRD pattern of pure $CsPbI_3$ shows several

https://dx.doi.org/10.1021/acs.jpcc.0c07983
J. Phys. Chem. C 2021, 125, 886–897

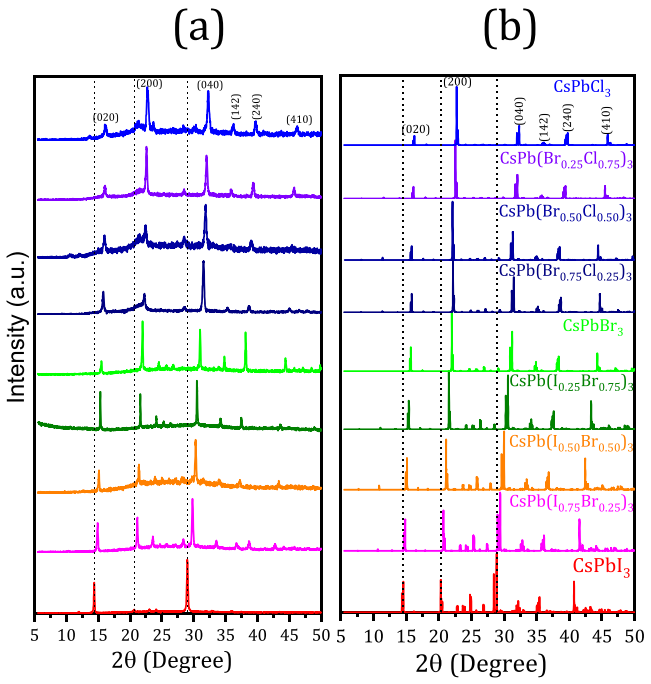

Figure 3. XRD patterns for $CsPb(I_{1-x}Br_x)_3$ and $CsPb(Br_{1-x}Cl_x)_3$ perovskites: (a) experimental and (b) theoretical.

diffraction peaks, specifically, peaks at 14.35°, 20.66°, 23.05°, 24.08°, 29.00°, 32.94°, and 35.96°. The pattern of pure $CsPbBr_3$ shows peaks at 15.54°, 22.00°, 24.54°, 25.71°, 26.80°, 30.99°, 34.83°, 38.17°, and 44.39°, whereas that of pure $CsPbCl_3$ shows peaks at 16.15°, 22.72°, 25.71°, 32.28°, 36.25°, 39.72°, and 46.26°. For additional details, see Figures S2−S4 and Table S1 in the Structural properties section of the Supporting Information.

Table S1 shows a comparison of the equilibrium lattice constants (a, b, and c) of $CsPbI_3$, $CsPbBr_3$, $CsPbCl_3$, and their mixed structures with those reported elsewhere.[49,54,58−72] Figure S3a,b shows the theoretical and experimental XRD patterns in the range $28.5° \leq 2\theta \leq 33°$. As noted in Table S1 and Figure S3a−d, the lattice parameters and unit-cell volume decrease in proportion to x, where the volume decreases according to the functions $V(x) = 2013.06474-432.10545x$ $(Å)^3$ and $V(x) = 1585.66658-152.98318x$ $(Å)^3$ for $CsPb(I_{1-x}Br_x)_3$ and $CsPb(Br_{1-x}Cl_x)_3$, respectively. $CsPbBr_3$ crystallizes in an orthorhombic perovskite phase[49−55] at room temperature, and $CsPbI_3$ is stable in an orthorhombic non-perovskite (yellow phase) at room temperature and changes to the cubic perovskite (black phase) when heated above ~310 °C.[7,55,71,73−75] $CsPbI_3$ is highly sensitive to the ambient atmosphere.[55,76] $CsPbI_3$ can easily transform into an orthorhombic non-perovskite[55,76] because of the relatively low tolerance factor (t = 0.80)[62,77,78] of this compound; in addition, when some portion of I^- anions are substituted with smaller Br^- anions, the tolerance factor increases (t = 0.92 for $CsPbBr_3$),[78] resulting in the formation of $CsPb(I_{1-x}Br_x)_3$ perovskites and retaining the orthorhombic composition.[62] Sutton et al.[55] and Yan et al.[79] have demonstrated that $CsPbI_2Br$ is more stable than pure $CsPbI_3$; our results show

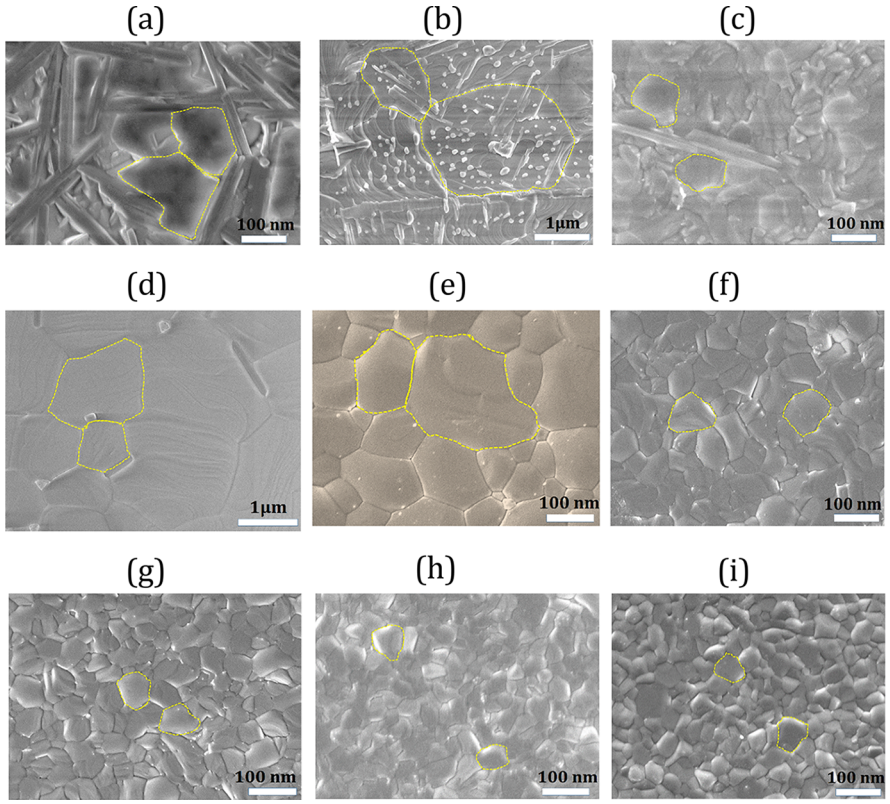

Figure 4. Scanning electron microscopy analysis of perovskite thin films prepared using a thermal evaporation system: (a) $CsPbI_3$, (b) $CsPb(I_{0.75}Br_{0.25})_3$, (c) $CsPb(I_{0.50}Br_{0.50})_3$, (d) $CsPb(I_{0.25}Br_{0.75})_3$, (e) $CsPbBr_3$, (f) $CsPb(Br_{0.75}Cl_{0.25})_3$, (g) $CsPb(Br_{0.50}Cl_{0.50})_3$, (h) $CsPb(Br_{0.25}Cl_{0.75})_3$, and (i) $CsPbCl_3$. The yellow dashed curves show the size of the grains. Sample scales (b) and (d) were selected at 1 μm because the two samples had large grain sizes (3.27 and 2.8 μm, respectively).

https://dx.doi.org/10.1021/acs.jpcc.0c07983
J. Phys. Chem. C 2021, 125, 886−897

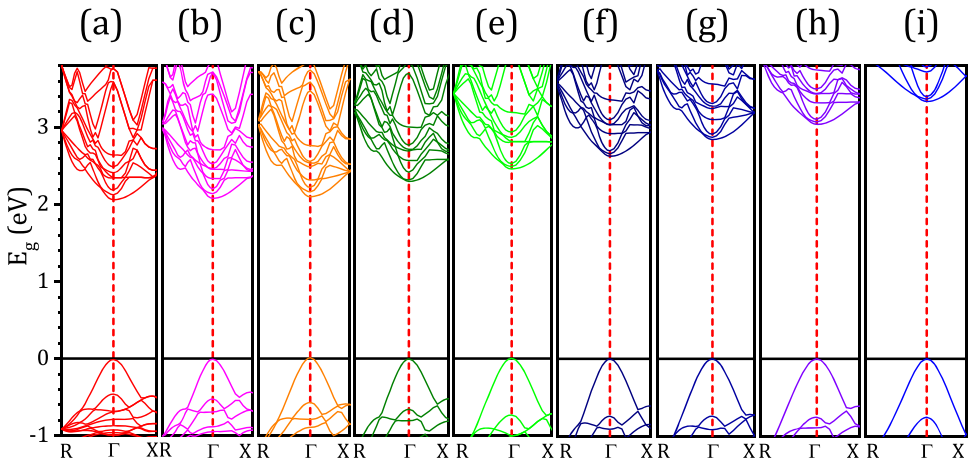

Figure 5. Band structures of the perovskite thin films, as calculated using the mBJ-GGA potential: (a) $CsPbI_3$, (b) $CsPb(I_{0.75}Br_{0.25})_3$, (c) $CsPb(I_{0.50}Br_{0.50})_3$, (d) $CsPb(I_{0.25}Br_{0.75})_3$, (e) $CsPbBr_3$, (f) $CsPb(Br_{0.75}Cl_{0.25})_3$, (g) $CsPb(Br_{0.50}Cl_{0.50})_3$, (h) $CsPb(Br_{0.25}Cl_{0.75})_3$, and (i) $CsPbCl_3$. The valence-band maximum is set as zero.

that, at x = 0.50, 0.75, and 1.00, the mixed perovskites exist as stable orthorhombic perovskite. The two new films, $CsPbI_3$ and $CsPb(I_{0.75}Br_{0.25})_3$, are susceptible to the ambient atmosphere and can be easily transformed into an orthorhombic nonperovskite after ∼2 h. We therefore recorded the XRD data immediately after the thin films were prepared (see Figure S5 in the Supporting Information).

The morphologies of the perovskite thin films were analyzed by SEM. The thin films prepared using the thermal evaporation system were found to be extremely uniform over the entire substrate, highly crystalline, pinhole-free, and composed of micrometer-sized grains in the range of 0.26−3.27 μm (Figure 4a−i and Supporting Information Figure S6). The thickness of the perovskite thin films was approximately 350−450 nm (Figure S7, Supporting Information).

First, the electronic structures were predicted using the mBJ-GGA potential. Because of the presence of the heavy element Pb, the SOC effect was included in the calculation of the electronic structure. Figure 5 shows the band structures calculated using the mBJ-GGA potentials without/with SOC. The band structures show direct-transition character at the Γ point. The calculated fundamental band gaps based on the mBJ-GGA potential are between 1.98 and 3.32 eV as shown in Table 1. These E_g results are close to our obtained experimental results and previously measured values.[59,70,80]

When the effect of SOC was included, the band gaps calculated using the mBJ-GGA potential become smaller than the experimental values; therefore, a correction was applied to the band gaps with the alloy formula[46−48]

$$\Delta E_g(A_{1-x}B_x) = (1 - x)\Delta E_g(A) + x\Delta E_g(B) \quad (1)$$

where $\Delta E_g(A_{1-x}B_x)$ is the correction for the band gap of $CsPb(I_{1-x}Br_x)_3$ or $CsPb(Br_{1-x}Cl_x)_3$ perovskites, $\Delta E_g(A)$ is the band gap correction for pure $CsPbI_3$ or $CsPbBr_3$, and $\Delta E_g(B)$ is the band gap correction for pure $CsPbBr_3$ or $CsPbCl_3$. Figure 6 shows the E_g values calculated using the mBJ-GGA, mBJ-GGA + SOC, and the corrected mBJ-GGA + SOC(C), where the E_g values are in excellent agreement with the experimental E_g values. (The experimental E_g values will be discussed later). The small differences between the theoretical and experimental values are attributed mainly to the different unit-cell sizes of the different mixed halides,[46] as depicted in the XRD patterns and the small 1 × 1 × 2 SC models.

Table 1. Band Gap E_g Values (eV) of $CsPb(I_{1-x}Br_x)_3$ and $CsPb(Br_{1-x}Cl_x)_3$ Perovskite, as Calculated Using the mBJ-GGA without/with SOC, Compared with Experimental Values

	this work				other work
compounds	mBJ-GGA	mBJ-GGA + SOC	mBJ-GGA + SOC (corrected)	exp.	DFT (exp.)
$CsPbI_3$	1.98	1.06	1.85	1.85	1.831[60,81]
					1.48[58]
					(1.75)[70]
					(1.73)[80]
$CsPb(I_{0.75}Br_{0.25})_3$	2.03	1.12	1.97	2.01	
$CsPb(I_{0.50}Br_{0.50})_3$	2.11	1.15	2.05	2.17	1.93[81]
					(1.97)[59]
$CsPb(I_{0.25}Br_{0.75})_3$	2.28	1.34	2.28	2.23	(2.17)[70]
$CsPbBr_3$	2.42	1.48	2.48	2.48	2.32[82]
					2.40[81]
					(2.38)[70]
					(2.39)[80]
$CsPb(Br_{0.75}Cl_{0.25})_3$	2.62	1.60	2.59	2.67	
$CsPb(Br_{0.50}Cl_{0.50})_3$	2.84	1.81	2.79	2.80	(2.72)[59]
$CsPb(Br_{0.25}Cl_{0.75})_3$	3.03	1.97	2.93	2.94	
$CsPbCl_3$	3.32	2.18	3.13	3.13	3.05[83]
					(2.91)[67]
					(2.78)[80]
					(2.98)[59]

The effective masses of an electron (m_e*) and a hole (m_h*) and reduced mass (μ) are important indices of the transport properties of photovoltaic materials.[83] They were calculated from the band structure and already used to calculate the exciton binding energy E_b of the compounds, (see Figure S8 and Table S2, Effective mass section, Supporting Information).

The optical properties of the films can be interpreted in view of the interaction between the incident photons and the semiconducting films.[84,85] The optical absorption spectrum can be used to obtain the band gap energy, which provides information about the band structure of semiconductors and nonmetallic materials.[84−86]

https://dx.doi.org/10.1021/acs.jpcc.0c07983
J. Phys. Chem. C 2021, 125, 886−897

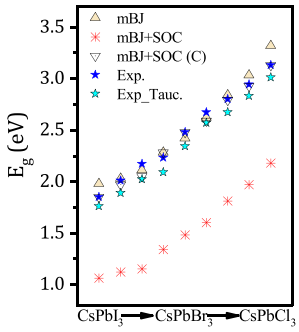

Figure 6. The E_g values of $CsPb(I_{1-x}Br_x)_3$ and $CsPb(Br_{1-x}Cl_x)_3$, as calculated using the mBJ-GGA potential with/without SOC. By applying the band gap correction, we obtained the mixed-ratio band gaps of inorganic mixed halide perovskite compared with the experimental results.

The optical absorbance spectra of the thin films were recorded in the UV−vis region of the electromagnetic spectrum, as shown in Figure 7a. The absorption comprises of three broad features: a sub-band gap absorption tail at low energy, followed by a strong exciton peak, followed by band-to-band transitions.[38,87] The onset of absorption shifts to shorter wavelengths (higher energy) with increasing Br^- and Cl^- concentrations, which leads to an increase in the band gap values from 1.82 eV for $CsPbI_3$ to 3.03 eV for $CsPbCl_3$ as shown in Table 2. We attempted to record all of the optical measurements immediately after the thin films were prepared (Figure S9a,b, optical properties, supporting information).

The investigated PL emission spectra of the pure and mixed halide films depend on the halide composition and their stoichiometric ratio, as depicted in Figure 7b. The spectra of the films show strong and narrow PL peaks at 700.56, 652.57, 623.23, 577.11, 524.80, 496.00, 469.69, 444.44, and 413.33 nm, as shown in Table 2. As shown in Figure 8, with decreasing atomic number of the halide elements from I to Br to Cl, the full width at half maximum (FWHM) and PL position decrease and the E_g values increase. As a consequence, the valence and conduction bands shift away from each other and the optical band gap increases. Halide elements with smaller atomic radii (0.10, 0.12, and 0.14 nm for Cl, Br, and I, respectively) in mixed films reduce the unit-cell dimensions and the covalency of the films.[59] The variation of the PL FWHM (approximately 12.42−32.36 nm) agrees well with the literature,[70,88−90] and these lower FWHM values suggest superior quality and good optical properties of the fabricated thin films by the thermal evaporation system.

Figure 9a,b shows the measured R and T over the wavelength range of 200−1000 nm having a resolution limit of 0.2 nm and a sampling interval of 2 nm. R and T measurements were carried out at 22 °C temperature for the spectral range of 0.2−3 mm with the incident beam making an angle of ∼6.9 ± 0.1° to the normal of the film external faces. The existence of oscillations is explained by the interference effect occurring due to the small thickness of the perovskite film t_f compared with large thickness of the glass substrate t_s ($t_f < t_s$) and the relative difference between substrate and film refractive indices n_s and n_f, respectively ($n_f \neq n_s$)[91,92] (see Figures S10 and S11, optical properties section, Supporting Information).

The optical absorption coefficient (α) was calculated from the optical absorption spectra using the formula[93,94]

$$\alpha = \frac{1}{t}\ln\left[\frac{(1-R)^2}{2T} + \left(\frac{(1-R)^4}{4T^2} + R^2\right)^{1/2}\right] \quad (2)$$

where t denotes the film thickness ($t \approx 350-450$ nm). Therefore, α spectra could be obtained using R and T measurements, as shown in Figure 10. The magnitude of α decreases with increasing Br and Cl contents. Parameter α shows high values (in the range 10^4-10^5 cm^{-1}), which indicates an improvement of the stacking of the layers of the perovskite thin films by the evaporation method. Our results are in broad agreement with results already published for similar materials.[95,96]

Figure S12 in the Supporting Information shows the experimental E_g values of perovskite thin films, as calculated using the well-known Tauc equation:[97−99]

$$\alpha h\nu = A(h\nu - E_g)^n \quad (3)$$

The E_g value increased from 1.76 for $CsPbI_3$ to 3.01 eV for $CsPbCl_3$ (ΔE_g = 1.25 eV) (see the Supporting Information, Optical properties section for more details). However, as in Figure 10, we noted that the exciton absorption dominates the absorption spectra near the band gap, which leads to the nonapplicability of eq 3. Because of the inaccuracy of the Tauc equation, we calculated the E_g value for the $CsPb(I_{1-x}Br_x)_3$ and $CsPb(Br_{1-x}Cl_x)_3$ perovskite thin films by evaluating the

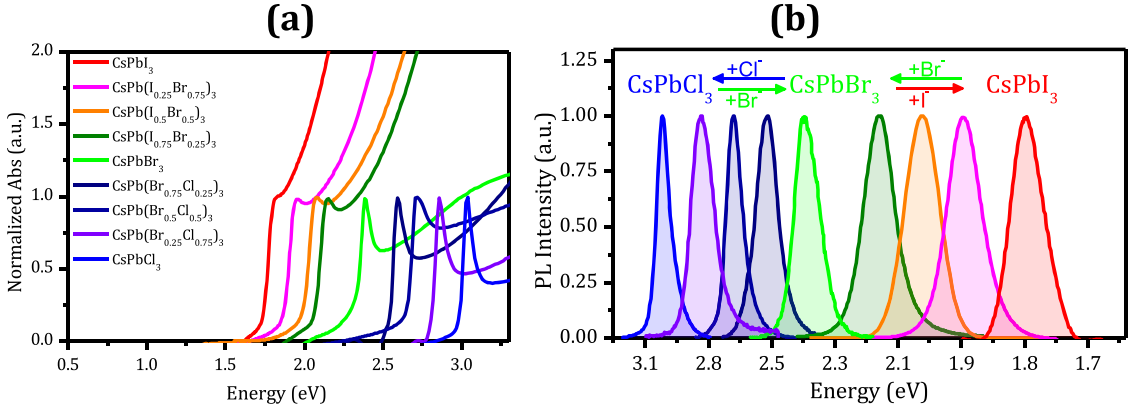

Figure 7. Normalized spectra of $CsPbI_3$, $CsPb(I_{0.75}Br_{0.25})_3$, $CsPb(I_{0.50}Br_{0.50})_3$, $CsPb(I_{0.25}Br_{0.75})_3$, $CsPbBr_3$, $CsPb(Br_{0.75}Cl_{0.25})_3$, $CsPb(Br_{0.50}Cl_{0.50})_3$, $CsPb(Br_{0.25}Cl_{0.75})_3$, and $CsPbCl_3$ thin films: (a) absorption and (b) emission spectra.

https://dx.doi.org/10.1021/acs.jpcc.0c07983
J. Phys. Chem. C 2021, 125, 886−897

Table 2. Optical Band Gap E_g Values, Exciton and PL Peak Positions, FWHMs of the Exciton and PL, and Urbach Energy of the $CsPb(I_{1-x}Br_x)_3$ and $CsPb(Br_{1-x}Cl_x)_3$ Perovskites

compounds	band gap E_g (eV)	exciton binding energy E_b (meV)	exciton peak (nm)	FWHM exciton peak (meV)	Urbach energy (meV)	PL peak (nm)	PL peak (eV)	FWHM of the PL peak (nm)
$CsPbI_3$	1.85 1.95[107]	45.73 39.44[DFT]	683 674[88]	100.10	76.92	700.56 696[88] 692[108]	1.77 1.87[109]	31.03 33[88]
$CsPb(I_{0.75}Br_{0.25})_3$	2.01	46.10 45.03[DFT]	637 661[88]	89.50	44.10	652.57 677[88] 640[89] 650[108]	1.91 2.08[109]	31.99 35[88,89]
$CsPb(I_{0.50}Br_{0.50})_3$	2.17 2.17[107]	46.35 45.39[DFT]	591 560[88] 600[89]	105.99	54.05	623.23 622[88]	2.00 2.14[109]	32.36 32[88] 38[89]
$CsPb(I_{0.25}Br_{0.75})_3$	2.23	55.97 55.12[DFT]	574 560[88]	89.55	57.47	577.11 581[88]	2.12 2.25[109]	28.87 27[88]
$CsPbBr_3$	2.48 2.48[107]	62.20 63.04[DFT]	512 500[88] 513[89]	82.55	60.53	524.80 517[88,90] 530[70]	2.36 2.43[109]	23.24 21[88] 20[89] 26[70] **23[90]
$CsPb(Br_{0.75}Cl_{0.25})_3$	2.67	67.87 50.44[DFT]	477	56.64	28.2	496	2.50	20.23
$CsPb(Br_{0.50}Cl_{0.50})_3$	2.80	68.00 67.69[DFT]	456	85.01	52.69	469.69	2.64	14.98
$CsPb(Br_{0.25}Cl_{0.75})_3$	2.94	76.65 74.76[DFT]	433	99.16	29.45	444.44	2.79	20.90
$CsPbCl_3$	3.13	95.23 96.73[DFT]	409	82.73	32.08	413.33	3.00	12.42

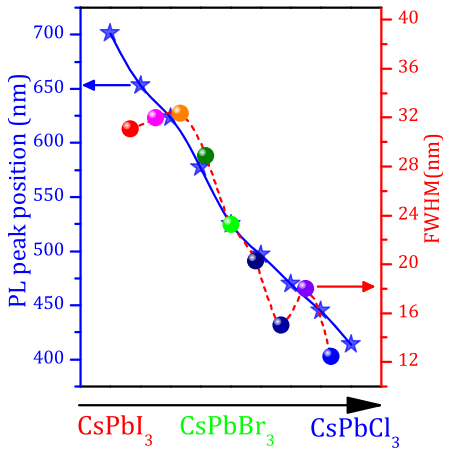

Figure 8. PL spectral peak positions and FWHM versus Br and Cl contents.

Coulomb field of the exciton, which is known as the Sommerfield factor, $S(E)$, where E represents the photon energy.[38] Here, we have taken into account the $S(E)$ to evaluate the absorption coefficient $\alpha(E)$ for the films using the following expression:[38,100,101]

$$\alpha(E) = X + \mathrm{conv}(Y \cdot Z) \tag{4}$$

where

$$X = \left(\frac{2}{\sqrt{2\pi}}\right)\cdot(E_b)^{3/2}\cdot\frac{A}{\sigma_1}\exp\left(-\frac{(E - E_g - E_b)^2}{2\,\sigma_1{}^2}\right) \tag{4a}$$

$$Y = \left(\frac{2}{\sqrt{2\pi}}\right)\cdot(E_b)^{3/2}\cdot\frac{B}{\sigma_2}\exp\left(-\frac{(E - E_g - E_b)^2}{2\,\sigma_2{}^2}\right) \tag{4b}$$

$$Z = (2\pi\cdot C\cdot(E - E_g)^{1/2}\cdot\theta(E - E_g))\cdot S(E) \tag{4c}$$

$$S(E) = \left(\frac{2\pi\sqrt{\frac{E_b}{E - E_g}}}{1 - \exp(-2\pi\sqrt{\frac{E_b}{E - E_g}})}\right) \tag{4d}$$

where A, B, and C are constants. The quantities E_b and E_g are the exciton binding energy and energy band gap, respectively; σ_1 and σ_2 are the FWHMs of the excitonic peaks. Conv(Y·Z) and $\theta(E - E_g)$ represent the convolution of the functions (Y, Z) and the Heaviside step function, respectively. In eq 4, the first term represents the exciton transition, where the exciton peak was taken to have a Gaussian peak shape with a width of σ_1, and the second term is due to the band-to-band transitions, including the $S(E)$ factor. The absorption was modeled according to inhomogeneous broadening by convolving eq 4 with FWHMs of ~100, ~82.55, and ~82.73 meV for pure $CsPbI_3$, $CsPbBr_3$, and $CsPbCl_3$, respectively. Figure 11 shows the deconvoluted absorption spectra for the exciton and band-to-band transitions. The excitonic and band-to-band absorptions with experimental absorption data (Table 2) shows the calculated band gaps and the exciton binding energy for the different compositions. Figure S13 in the Supporting Information shows the excitonic and band-to-band absorptions with experimental data for all of the investigated inorganic thin films.

https://dx.doi.org/10.1021/acs.jpcc.0c07983
J. Phys. Chem. C 2021, 125, 886−897

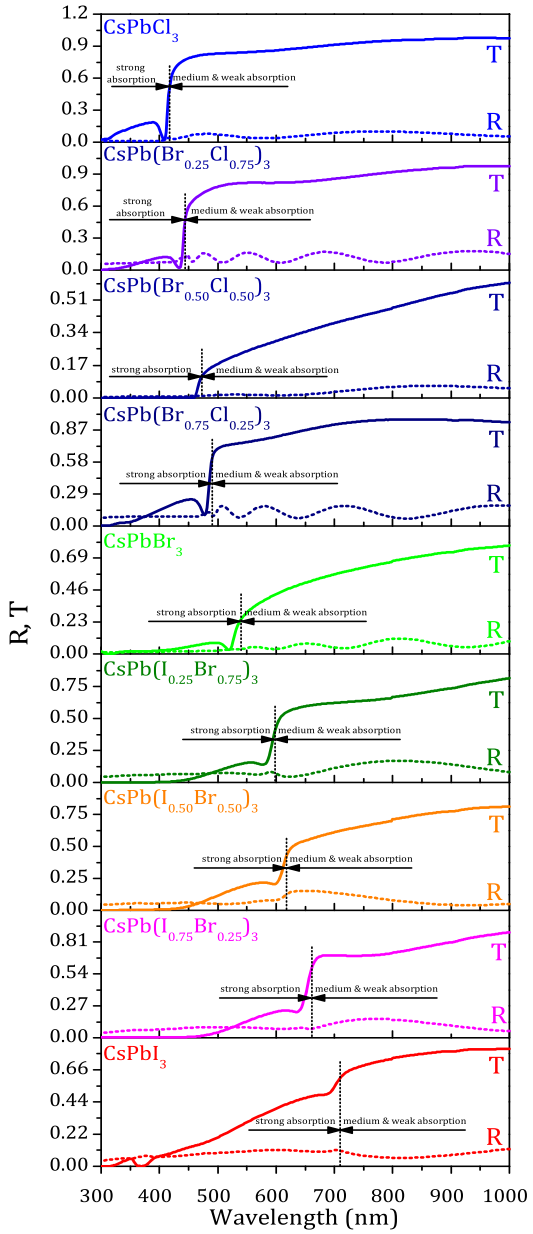

Figure 9. Reflectance R and transmittance T spectra of CsPb$(I_{1-x}Br_x)_3$ and CsPb$(Br_{1-x}Cl_x)_3$ perovskite thin films.

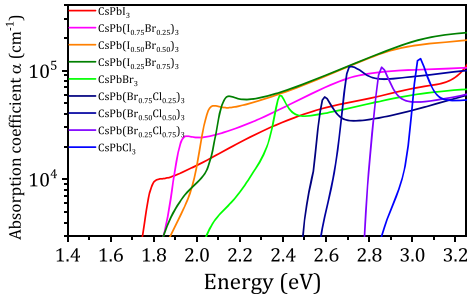

Figure 10. Absorption coefficient spectra of the studied CsPb$(I_{1-x}Br_x)_3$ and CsPb$(Br_{1-x}Cl_x)_3$ thin films.

The variation of E_g values with the Br and Cl concentrations can be expressed as follows:[59,102−105]

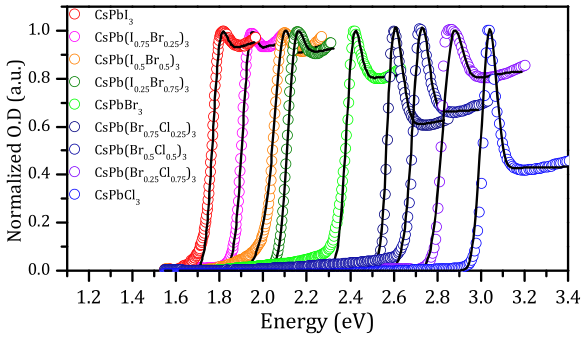

Figure 11. Normalized optical density vs energy for CsPb$(I_{1-x}Br_x)_3$ and CsPb$(Br_{1-x}Cl_x)_3$ perovskite thin films. The black solid lines represent the fitting using eq 4.

$$E_g^{CsPb(A_{1-x}B_x)_3} = xE_g(B) + (1-x)E_g(A) - x(1-x)b \quad (5)$$

where x is the Br or Cl content and b is the bowing parameter. Equation 5 represents the E_g bowing effect with increasing Br/I and Cl/Br ratios in CsPb$(I_{1-x}Br_x)_3$ and CsPb$(Br_{1-x}Cl_x)_3$, respectively.

Figure S14a,b in the Supporting Information shows the experimental and theoretical band gaps, E_g, of the all-inorganic perovskite thin films. The total bowing parameters (b) were determined by fitting the nonlinear variation E_g as Br and Cl concentrations x using a second-order polynomial. The small bowing parameters b = 0.10 and 0.31 eV correspond to the experimental and theoretical E_g, respectively, of CsPb$(I_{1-x}Br_x)_3$, whereas b = 0.011 and 0.17 eV correspond to the experimental and theoretical E_g, respectively, for CsPb$(Br_{1-x}Cl_x)_3$. These bowing parameters are substantially smaller than those for previous works (i.e., b = 0.33 eV[105] for organic $CH_3NH_3Pb(I_{1-x}Br_x)_3$ perovskites, b = 0.29 eV[59] for one-dimensional inorganic CsPb$(I_{1-x}Br_x)_3$, $b \approx$ 0.477 eV[106] for the conventional semiconductor $In_xGa_{1-x}As$, and $b \approx$ 0.45 eV[104] for $Zn_xCd_{1-x}Se$ nanowires). See eqs S4−S11, Supporting Information, for more details.

To gain further insight into the optical properties, we plotted the logarithmic optical absorption coefficient as a function of the energy to investigate the Urbach energy (E_U) (as illustrated in Figure S15a−i and Figure S16 in the Supporting Information). The E_U values were derived from the Urbach tail near the optical band edge; α follows the Urbach empirical rule according to the equation[84,110−113]

$$\ln(\alpha) = \ln(\alpha_0) + \left(\frac{h\nu}{E_U}\right) \quad (6)$$

where α_0 is constant. Figure S15 clearly shows that the E_U fluctuates between 28 and 77 meV, which means that the minimum E_U correlates to fewer trap states in the thin film, which would lead to slower recombination.[97,111−113]

The absorption of light waves and the optical dielectric parameters of any medium depends mainly on the extinction coefficient (k) and can be calculated using the formula[84,114,115]

$$k = \frac{\alpha\lambda}{4\pi} \quad (7)$$

Figure 12c shows that the k curves for $CsPbI_3$, CsPb$(I_{0.50}Br_{0.50})_3$, $CsPbBr_3$, CsPb$(Br_{0.50}Cl_{0.50})_3$, and $CsPbCl_3$ decrease slightly in intensity with increasing Br and Cl

https://dx.doi.org/10.1021/acs.jpcc.0c07983
J. Phys. Chem. C 2021, 125, 886−897

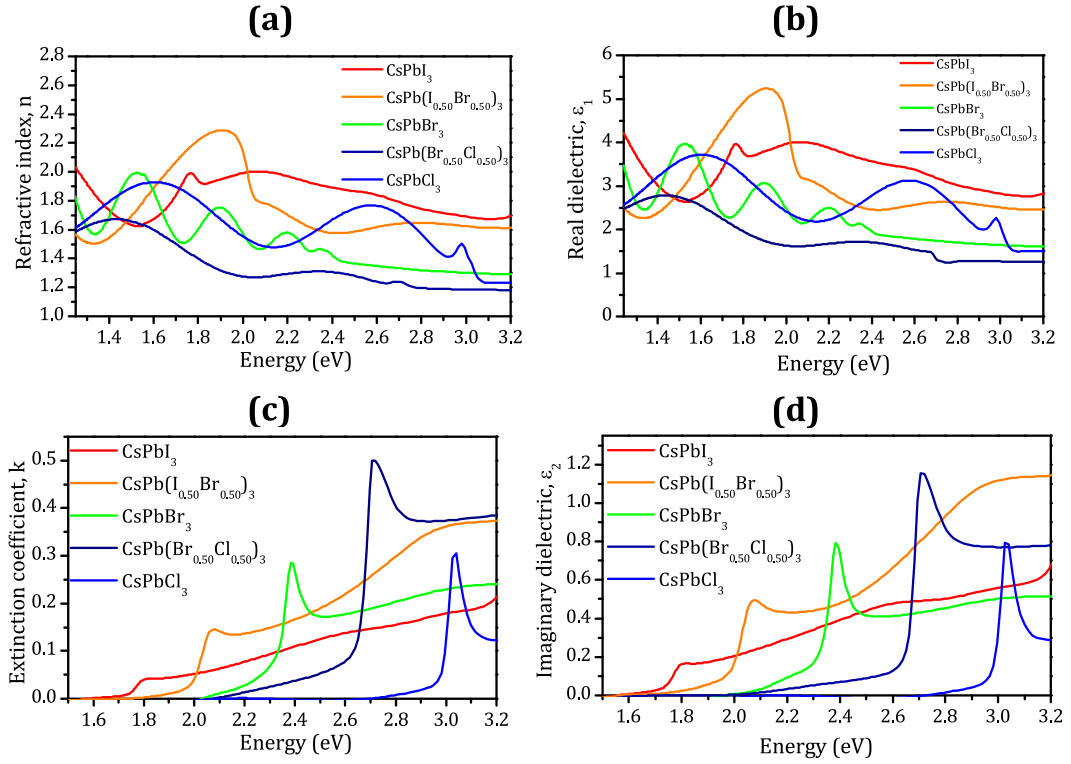

Figure 12. Properties of the $CsPbI_3$, $CsPb(I_{0.50}Br_{0.50})_3$, $CsPbBr_3$, $CsPb(Br_{0.50}Cl_{0.50})_3$, and $CsPbCl_3$ thin films: (a) refractive index, (b) real dielectric constant, (c) extinction coefficient, and (d) the imaginary dielectric constant.

concentrations. Another important property related to the extent of the influence of matter by electromagnetic waves is the refractive index (n), which can be computed using the Kramer–Kroning's formula:[85,94,114,116−120]

$$n = \left(\frac{1 + \mathrm{R}}{1 - \mathrm{R}}\right) + \sqrt{\frac{4R}{(1 - \mathrm{R})^2} - k^2} \tag{8}$$

where R is the reflectance of the thin films.

The n curves according to the energy are presented in Figure 12a, where the n values fluctuate in the visible range between 1.5 and 6 eV. The higher n values indicate a decrease in the speed of light or a decrease in the spread of electromagnetic waves through this material.[85]

The optical properties can be described using the complex dielectric function ε that exhibits two parts: a real part ε_1 and an imaginary component ε_2. The real and imaginary parts of the dielectric constant were calculated using the equations[114,116]

$$\varepsilon_1 = n^2 - k^2 \tag{9}$$

$$\varepsilon_2 = 2nk \tag{10}$$

The dielectric constants depend upon n and K. Figure 12b,d shows that ε_1 and ε_2 decreased with increasing Br and Cl contents.

5. CONCLUSIONS

High-quality inorganic $CsPb(I_{1-x}Br_x)_3$ and $CsPb(Br_{1-x}Cl_x)_3$ perovskite thin films were prepared using a thermal evaporation technique. Experimental measurements and first-principles calculations (using the highly accurate mBJ-GGA method) were carried out to fully elucidate the structural, electronic, and optical properties of the prepared films at room temperature. Theoretical and experimental XRD patterns were discussed, and they showed that the peaks shifted toward higher 2θ values in the progression from $CsPbI_3$ to $CsPbCl_3$. The band gap of the thin-film perovskites were in excellent agreement with theoretical and corrected band gaps obtained using the most accurate mBJ-GGA potential. Dominant excitonic effects on the onset of optical absorption led us to explicitly account for the enhancement of absorption through the Sommerfeld factor. The fitting was applied to the absorption spectra, which enabled us to extract the electronic band gap and the exciton binding energy correctly. The experimental results were correlated with the theory of first-principles and provided insights into the lattice parameters, electronic structure, excitonic binding energy, dielectric constant, and reduced effective mass of the carriers. With increasing concentrations (x) of Br and Cl, the E_b value increased because of a decrease in the dielectric constant and the almost constant value of μ at ~0.051m_e. The Urbach energy E_U was calculated and found to fluctuate between 28 and 77 meV.

■ ASSOCIATED CONTENT

Supporting Information

The Supporting Information is available free of charge at https://pubs.acs.org/doi/10.1021/acs.jpcc.0c07983.

More details of structural, electronic, and optical properties of $CsPb(Br_{1-x}Cl_x)_3$ perovskite thin films (PDF)

■ AUTHOR INFORMATION

Corresponding Authors

Hamid M. Ghaithan − *Physics and Astronomy Department, College of Science, King Saud University, Riyadh 11451,*

https://dx.doi.org/10.1021/acs.jpcc.0c07983
J. Phys. Chem. C 2021, 125, 886−897

Saudi Arabia; Physics Department, College of Education and linguistics, Amran University, Amran 2915, Yemen; orcid.org/0000-0001-5126-4477; Phone: +966 532257491; Email: hghaithan@ksu.edu.sa

Saif M. H. Qaid − *Physics and Astronomy Department, College of Science, King Saud University, Riyadh 11451, Saudi Arabia;* orcid.org/0000-0001-8958-8960; Email: sqaid@ksu.edu.sa

Zeyad A. Alahmed − *Physics and Astronomy Department, College of Science, King Saud University, Riyadh 11451, Saudi Arabia*; Email: zalahmed@ksu.edu.sa

Abdullah S. Aldwayyan − *Physics and Astronomy Department, College of Science and King Abdullah Institute for Nanotechnology, King Saud University, Riyadh 11451, Saudi Arabia; K.A.CARE Energy Research and Innovation Center at Riyadh, Riyadh 11454, Saudi Arabia*; Email: dwayyan@ksu.edu.sa

Authors

Mahmoud Hezam − *King Abdullah Institute for Nanotechnology, King Saud University, Riyadh 11451, Saudi Arabia*

Andreas Lyras − *Physics and Astronomy Department, College of Science, King Saud University, Riyadh 11451, Saudi Arabia*

Mabrook Amer − *Electrochemical Sciences Research Chair (ESRC), Chemistry Department, College of Science, King Saud University, Riyadh 11451, Saudi Arabia; K.A.CARE Energy Research and Innovation Center at Riyadh, Riyadh 11454, Saudi Arabia*

Complete contact information is available at: https://pubs.acs.org/10.1021/acs.jpcc.0c07983

Notes

The authors declare no competing financial interest.

■ ACKNOWLEDGMENTS

The authors extend their appreciation to the Deputyship for Research & Innovation, "Ministry of Education" in Saudi Arabia for funding this research work through the project number IFKSURG-265.

■ REFERENCES

(1) Zhang, Y.; Luo, L.; Hua, J.; Wang, C.; Huang, F.; Zhong, J.; Peng, Y.; Ku, Z.; Cheng, Y.-B. Moisture Assisted $CsPbBr_3$ Film Growth for High-Efficiency, All-Inorganic Solar Cells Prepared by a Multiple Sequential Vacuum Deposition Method. *Mater. Sci. Semicond. Process.* **2019**, *98*, 39−43.

(2) Lee, M. M.; Teuscher, J.; Miyasaka, T.; Murakami, T. N.; Snaith, H. J. Efficient Hybrid Solar Cells Based on Meso-Superstructured Organometal Halide Perovskites. *Science* **2012**, *338*, 643−647.

(3) Kim, H.-S.; Lee, C.-R.; Im, J.-H.; Lee, K.-B.; Moehl, T.; Marchioro, A.; Moon, S.-J.; Humphry-Baker, R.; Yum, J.-H.; Moser, J. E.; et al. Lead Iodide Perovskite Sensitized All-Solid-State Submicron Thin Film Mesoscopic Solar Cell with Efficiency Exceeding 9%. *Sci. Rep.* **2012**, *2*, 591.

(4) Kojima, A.; Teshima, K.; Shirai, Y.; Miyasaka, T. Organometal Halide Perovskites as Visible-Light Sensitizers for Photovoltaic Cells. *J. Am. Chem. Soc.* **2009**, *131*, 6050−6051.

(5) Yuan, H.; Zhao, Y.; Duan, J.; Wang, Y.; Yang, X.; Tang, Q. All-Inorganic $CsPbBr_3$ Perovskite Solar Cell with 10.26% Efficiency by Spectra Engineering. *J. Mater. Chem. A* **2018**, *6*, 24324−24329.

(6) Poli, I.; Baker, J.; McGettrick, J.; De Rossi, F.; Eslava, S.; Watson, T.; Cameron, P. J. Screen Printed Carbon $CsPbBr_3$ Solar Cells with High Open-Circuit Photovoltage. *J. Mater. Chem. A* **2018**, *6*, 18677−18686.

(7) Wang, K.; Jin, Z.; Liang, L.; Bian, H.; Bai, D.; Wang, H.; Zhang, J.; Wang, Q.; Liu, S. All-Inorganic Cesium Lead Iodide Perovskite Solar Cells with Stabilized Efficiency beyond 15%. *Nat. Commun.* **2018**, *9*, 4544.

(8) Wu, T.; Wang, Y.; Dai, Z.; Cui, D.; Wang, T.; Meng, X.; Bi, E.; Yang, X.; Han, L. Efficient and Stable $CsPbI_3$ Solar Cells via Regulating Lattice Distortion with Surface Organic Terminal Groups. *Adv. Mater.* **2019**, *31*, 1900605−1900609.

(9) Zhang, L.; Yang, X.; Jiang, Q.; Wang, P.; Yin, Z.; Zhang, X.; Tan, H.; Yang, Y. M.; Wei, M.; Sutherland, B. R.; Sargent, E. H.; You, J. Ultra-Bright and Highly Efficient Inorganic Based Perovskite Light-Emitting Diodes. *Nat. Commun.* **2017**, *8*, 1−8.

(10) Lin, K.; Xing, J.; Quan, L. N.; de Arquer, F. P. G.; Gong, X.; Lu, J.; Xie, L.; Zhao, W.; Zhang, D.; Yan, C.; et al. Perovskite Light-Emitting Diodes with External Quantum Efficiency Exceeding 20 per Cent. *Nature*. Springer US 2018, pp. 245−248.

(11) Li, Z.; Chen, Z.; Yang, Y.; Xue, Q.; Yip, H. L.; Cao, Y. Modulation of Recombination Zone Position for Quasi-Two-Dimensional Blue Perovskite Light-Emitting Diodes with Efficiency Exceeding 5%. *Nat. Commun.* **2019**, *10*, 1027.

(12) Liu, Y.; Cui, J.; Du, K.; Tian, H.; He, Z.; Zhou, Q.; Yang, Z.; Deng, Y.; Chen, D.; Zuo, X.; et al. Efficient Blue Light-Emitting Diodes Based on Quantum-Confined Bromide Perovskite Nanostructures. *Nature Photonics*. Springer US 2019, pp. 760−764.

(13) Yuan, Z.; Miao, Y.; Hu, Z.; Xu, W.; Kuang, C.; Pan, K.; Liu, P.; Lai, J.; Sun, B.; Wang, J.; et al. Unveiling the Synergistic Effect of Precursor Stoichiometry and Interfacial Reactions for Perovskite Light-Emitting Diodes. *Nat. Commun.* **2019**, *10*, 2818.

(14) Miao, Y.; Ke, Y.; Wang, N.; Zou, W.; Xu, M.; Cao, Y.; Sun, Y.; Yang, R.; Wang, Y.; Tong, Y.; et al. Stable and Bright Formamidinium-Based Perovskite Light-Emitting Diodes with High Energy Conversion Efficiency. *Nat. Commun.* **2019**, *10*, 3624.

(15) Zhang, Q.; Tavakoli, M. M.; Gu, L.; Zhang, D.; Tang, L.; Gao, Y.; Guo, J.; Lin, Y.; Leung, S.-F.; Poddar, S.; et al. Efficient Metal Halide Perovskite Light-Emitting Diodes with Significantly Improved Light Extraction on Nanophotonic Substrates. *Nat. Commun.* **2019**, *10*, 727.

(16) Matsushima, T.; Bencheikh, F.; Komino, T.; Leyden, M. R.; Sandanayaka, A. S. D.; Qin, C.; Adachi, C. High Performance from Extraordinarily Thick Organic Light-Emitting Diodes. *Nature*. Springer US 2019, pp. 502−506.

(17) Song, J.; Li, J.; Li, X.; Xu, L.; Dong, Y.; Zeng, H. Quantum Dot Light-Emitting Diodes Based on Inorganic Perovskite Cesium Lead Halides ($CsPbX_3$). *Adv. Mater.* **2015**, *27*, 7162−7167.

(18) Bekenstein, Y.; Koscher, B. A.; Eaton, S. W.; Yang, P.; Alivisatos, A. P. Highly Luminescent Colloidal Nanoplates of Perovskite Cesium Lead Halide and Their Oriented Assemblies. *J. Am. Chem. Soc.* **2015**, *137*, 16008−16011.

(19) Yakunin, S.; Protesescu, L.; Krieg, F.; Bodnarchuk, M. I.; Nedelcu, G.; Humer, M.; De Luca, G.; Fiebig, M.; Heiss, W.; Kovalenko, M. V. Low-Threshold Amplified Spontaneous Emission and Lasing from Colloidal Nanocrystals of Caesium Lead Halide Perovskites Lead Halide Perovskites. *Nat. Commun.* **2015**, *6*, 8056.

(20) Akkerman, Q. A.; Motti, S. G.; Srimath Kandada, A. R.; Mosconi, E.; D'Innocenzo, V.; Bertoni, G.; Marras, S.; Kamino, B. A.; Miranda, L.; De Angelis, F.; et al. Solution Synthesis Approach to Colloidal Cesium Lead Halide Perovskite Nanoplatelets with Monolayer-Level Thickness Control. *J. Am. Chem. Soc.* **2016**, *138*, 1010−1016.

(21) Tan, Z. K.; Moghaddam, R. S.; Lai, M. L.; Docampo, P.; Higler, R.; Deschler, F.; Price, M.; Sadhanala, A.; Pazos, L. M.; Credgington, D.; et al. Bright Light-Emitting Diodes Based on Organometal Halide Perovskite. *Nat. Nanotechnol.* **2014**, *9*, 687−692.

(22) Stranks, S. D.; Snaith, H. J. Metal-Halide Perovskites for Photovoltaic and Light-Emitting Devices. *Nat. Nanotechnol.* **2015**, *10*, 391−402.

(23) Cho, H.; Jeong, S.-H.; Park, M.-H.; Kim, Y.-H.; Wolf, C.; Lee, C.-L.; Heo, J. H.; Sadhanala, A.; Myoung, N. S.; Yoo, S.; Im, S. H.; Friend, R. H.; Lee, T.-W. Overcoming the Electroluminescence Efficiency Limitations of Perovskite Light-Emitting Diodes. *Science* **2015**, *350*, 1222−1225.
(24) Veldhuis, S. A.; Boix, P. P.; Yantara, N.; Li, M.; Sum, T. C.; Mathews, N.; Mhaisalkar, S. G. Perovskite Materials for Light-Emitting Diodes and Lasers. *Adv. Mater.* **2016**, 6804−6834.
(25) Deschler, F.; Price, M.; Pathak, S.; Klintberg, L. E.; Jarausch, D. D.; Higler, R.; Hüttner, S.; Leijtens, T.; Stranks, S. D.; Snaith, H. J.; et al. High Photoluminescence Efficiency and Optically Pumped Lasing in Solution-Processed Mixed Halide Perovskite Semiconductors. *J. Phys. Chem. Lett.* **2014**, *5*, 1421−1426.
(26) Xing, G.; Mathews, N.; Lim, S. S.; Yantara, N.; Liu, X.; Sabba, D.; Grätzel, M.; Mhaisalkar, S.; Sum, T. C. Low-Temperature Solution-Processed Wavelength-Tunable Perovskites for Lasing. *Nat. Mater.* **2014**, *13*, 476−480.
(27) Dou, L.; Yang, Y. M.; You, J.; Hong, Z.; Chang, W.-H.; Li, G.; Yang, Y. Solution-Processed Hybrid Perovskite Photodetectors with High Detectivity. *Nat. Commun.* **2014**, *5*, 1−6.
(28) Xie, C.; You, P.; Liu, Z.; Li, L.; Yan, F. Ultrasensitive Broadband Phototransistors Based on Perovskite/Organic-Semiconductor Vertical Heterojunctions. *Light: Sci. Appl.* **2017**, *6*, e17023−e17023.
(29) Ball, J. M.; Lee, M. M.; Hey, A.; Snaith, H. J. Low-Temperature Processed Meso-Superstructured to Thin-Film Perovskite Solar Cells. *Energy Environ. Sci.* **2013**, *6*, 1739−1743.
(30) Zheng, L.; Zhang, D.; Ma, Y.; Lu, Z.; Chen, Z.; Wang, S.; Xiao, L.; Gong, Q. Morphology Control of the Perovskite Films for Efficient Solar Cells. *Dalton Transactions*; Royal Society of Chemistry: 2015, pp. 10582−10593.
(31) Zhao, Y.; Zhu, K. Organic-Inorganic Hybrid Lead Halide Perovskites for Optoelectronic and Electronic Applications. *Chem. Soc. Rev.* **2016**, *45*, 655−689.
(32) Dang, Y.; Ju, D.; Wang, L.; Tao, X. Recent Progress in the Synthesis of Hybrid Halide Perovskite Single Crystals. *CrystEngComm* **2016**, *18*, 4476−4484.
(33) Ávila, J.; Momblona, C.; Boix, P. P.; Sessolo, M.; Bolink, H. J. Vapor-Deposited Perovskites: The Route to High-Performance Solar Cell Production? *Joule* **2017**, *1*, 431−442.
(34) Park, C.-G.; Choi, W.-G.; Na, S.; Moon, T. All-Inorganic Perovskite $CsPbI_2Br$ Through Co-Evaporation for Planar Heterojunction Solar Cells. *Electron. Mater. Lett.* **2019**, *15*, 56−60.
(35) Sessolo, M.; Momblona, C.; Gil-Escrig, L.; Bolink, H. J. Photovoltaic Devices Employing Vacuum-Deposited Perovskite Layers. *MRS Bull.* **2015**, *40*, 660−666.
(36) Shen, P.-S.; Chiang, Y.-H.; Li, M.-H.; Guo, T.-F.; Chen, P. Research Update: Hybrid Organic-Inorganic Perovskite (HOIP) Thin Films and Solar Cells by Vapor Phase Reaction. *APL Mater.* **2016**, *4*, No. 091509.
(37) Liu, C.; Fan, J.; Zhang, X.; Shen, Y.; Yang, L.; Mai, Y. Hysteretic Behavior upon Light Soaking in Perovskite Solar Cells Prepared via Modified Vapor-Assisted Solution Process. *ACS Appl. Mater. Interfaces* **2015**, *7*, 9066−9071.
(38) Kumawat, N. K.; Dey, A.; Kumar, A.; Gopinathan, S. P.; Narasimhan, K. L.; Kabra, D. Band Gap Tuning of $CH_3NH_3Pb(Br_{1-x}Cl_x)_3$ Hybrid Perovskite for Blue Electroluminescence. *ACS Appl. Mater. Interfaces* **2015**, *7*, 13119−13124.
(39) Kohn, W.; Sham, L. J. Self-Consistent Equations Including Exchange and Correlation Effects. *Phys. Rev.* **1965**, *140*, A1133.
(40) Parr, R. G. Density Functional Theory of Atoms and Molecules. In *Horizons of Quantum Chemistry*; Springer: 1980; pp. 5−15, DOI: 10.1007/978-94-009-9027-2_2.
(41) Perdew, J. P.; Ruzsinszky, A.; Csonka, G. I.; Vydrov, O. A.; Scuseria, G. E.; Constantin, L. A.; Zhou, X.; Burke, K. Restoring the Density-Gradient Expansion for Exchange in Solids and Surfaces. *Phys. Rev. Lett.* **2008**, *100*, 136406.
(42) Momma, K.; Izumi, F. *VESTA 3* for Three-Dimensional Visualization of Crystal, Volumetric and Morphology Data. *J. Appl. Crystallogr.* **2011**, *44*, 1272−1276.
(43) Narsimha Rao, E.; Vaitheeswaran, G.; Reshak, A. H.; Auluck, S. Role of Spin-Orbit Interaction on the Nonlinear Optical Response of $CsPbCO_3F$ Using DFT. *Phys. Chem. Chem. Phys.* **2017**, *19*, 31255−31266.
(44) Even, J.; Pedesseau, L.; Jancu, J. M.; Katan, C. Importance of Spin-Orbit Coupling in Hybrid Organic/Inorganic Perovskites for Photovoltaic Applications. *J. Phys. Chem. Lett.* **2013**, *4*, 2999−3005.
(45) Wu, Z.; Cohen, R. E. More Accurate Generalized Gradient Approximation for Solids. *Phys. Rev. B: Condens. Matter Mater. Phys.* **2006**, *73*, 235116.
(46) Su, Y.; Chen, X.; Ji, W.; Zeng, Q.; Ren, Z.; Su, Z.; Liu, L. Highly Controllable and Efficient Synthesis of Mixed-Halide $CsPbX_3$ (X = Cl, Br, I) Perovskite QDs toward the Tunability of Entire Visible Light. *ACS Appl. Mater. Interfaces* **2017**, *9*, 33020−33028.
(47) Chen, X.; Han, D.; Su, Y.; Zeng, Q.; Liu, L.; Shen, D. Structural and Electronic Properties of Inorganic Mixed Halide Perovskites. *Phys. Status Solidi RRL* **2018**, *12*, 1800193.
(48) Yin, W.-J.; Yan, Y.; Wei, S.-H. Anomalous Alloy Properties in Mixed Halide Perovskites. *J. Phys. Chem. Lett.* **2014**, *5*, 3625−3631.
(49) MØLLER, C. K. Crystal Structure and Photoconductivity of Cæsium Plumbohalides. *Nature* **1958**, *182*, 1436.
(50) Rodová, M.; Brožek, J.; Knížek, K.; Nitsch, K. Phase Transitions in Ternary Caesium Lead Bromide. *J. Therm. Anal. Calorim.* **2003**, *71*, 667−673.
(51) Kirschner, M. S.; Diroll, B. T.; Guo, P.; Harvey, S. M.; Helweh, W.; Flanders, N. C.; Brumberg, A.; Watkins, N. E.; Leonard, A. A.; Evans, A. M.; et al. Photoinduced, Reversible Phase Transitions in All-Inorganic Perovskite Nanocrystals. *Nat. Commun.* **2019**, *10*, 504.
(52) Dos Reis, R.; Yang, H.; Ophus, C.; Ercius, P.; Bizarri, G.; Perrodin, D.; Shalapska, T.; Bourret, E.; Ciston, J.; Dahmen, U. Determination of the Structural Phase and Octahedral Rotation Angle in Halide Perovskites. *Appl. Phys. Lett.* **2018**, *112*, No. 071901.
(53) Møller, C. K. The Structure of Perovskite-Like Cæsium Plumbo Trihalides. *Mater. Fys. Medd. Dan. Vid. Selsk* **1959**, *32*, 1−27.
(54) Stoumpos, C. C.; Malliakas, C. D.; Peters, J. A.; Liu, Z.; Sebastian, M.; Im, J.; Chasapis, T. C.; Wibowo, A. C.; Chung, D. Y.; Freeman, A. J.; et al. Crystal Growth of the Perovskite Semiconductor $CsPbBr_3$: A New Material for High-Energy Radiation Detection. *Cryst. Growth Des.* **2013**, *13*, 2722−2727.
(55) Sutton, R. J.; Eperon, G. E.; Miranda, L.; Parrott, E. S.; Kamino, B. A.; Patel, J. B.; Hörantner, M. T.; Johnston, M. B.; Haghighirad, A. A.; Moore, D. T.; Snaith, H. J. Bandgap-Tunable Cesium Lead Halide Perovskites with High Thermal Stability for Efficient Solar Cells. *Adv. Energy Mater.* **2016**, *6*, 1502458.
(56) Zhang, M.; Zheng, Z.; Fu, Q.; Chen, Z.; He, J.; Zhang, S.; Chen, C.; Luo, W. Synthesis and Single Crystal Growth of Perovskite Semiconductor $_{CsPbBr3}$. *J. Cryst. Growth* **2018**, *484*, 37−42.
(57) Bertolotti, F.; Protesescu, L.; Kovalenko, M. V.; Yakunin, S.; Cervellino, A.; Billinge, S. J. L.; Terban, M. W.; Pedersen, J. S.; Masciocchi, N.; Guagliardi, A. Coherent Nanotwins and Dynamic Disorder in Cesium Lead Halide Perovskite Nanocrystals. *ACS Nano* **2017**, *11*, 3819−3831.
(58) Xiao, Z.; Yan, Y. Progress in Theoretical Study of Metal Halide Perovskite Solar Cell Materials. *Adv. Energy Mater.* **2017**, *7*, 1701136.
(59) Paul, T.; Chatterjee, B. K.; Maiti, S.; Sarkar, S.; Besra, N.; Das, B. K.; Panigrahi, K. J.; Thakur, S.; Ghorai, U. K.; Chattopadhyay, K. K. Tunable Cathodoluminescence over the Entire Visible Window from All-Inorganic Perovskite $CsPbX_3$ 1D Architecture. *J. Mater. Chem. C* **2018**, *6*, 3322−3333.
(60) Ray, D.; Clark, C.; Pham, H. Q.; Borycz, J.; Holmes, R. J.; Aydil, E. S.; Gagliardi, L. Computational Study of Structural and Electronic Properties of Lead-Free $CsMI_3$ Perovskites (M = Ge, Sn, Pb, Mg, Ca, Sr, and Ba). *J. Phys. Chem. C* **2018**, *122*, 7838−7848.
(61) Sutton, R. J.; Filip, M. R.; Haghighirad, A. A.; Sakai, N.; Wenger, B.; Giustino, F.; Snaith, H. J. Cubic or Orthorhombic?

Revealing the Crystal Structure of Metastable Black-Phase $CsPbI_3$ by Theory and Experiment. *ACS Energy Lett.* **2018**, *3*, 1787−1794.
(62) Zhou, Y.; Zhao, Y. Chemical Stability and Instability of Inorganic Halide Perovskites. *Energy Environ. Sci.* **2019**, *12*, 1495−1511.
(63) Trots, D. M.; Myagkota, S. V. High-Temperature Structural Evolution of Caesium and Rubidium Triiodoplumbates. *J. Phys. Chem. Solids* **2008**, *69*, 2520−2526.
(64) Protesescu, L.; Yakunin, S.; Bodnarchuk, M. I.; Krieg, F.; Caputo, R.; Hendon, C. H.; Yang, R. X.; Walsh, A.; Kovalenko, M. V. Nanocrystals of Cesium Lead Halide Perovskites ($CsPbX_3$, X = Cl, Br, and I): Novel Optoelectronic Materials Showing Bright Emission with Wide Color Gamut. *Nano Lett.* **2015**, *15*, 3692−3696.
(65) Ghaithan, H. M.; Alahmed, Z. A.; Qaid, S. M. H.; Hezam, M.; Aldwayyan, A. S. Density Functional Study of Cubic, Tetragonal, and Orthorhombic $CsPbBr_3$ Perovskite. *ACS Omega* **2020**, *5*, 7468−7480.
(66) Tomanová, K.; Čuba, V.; Brik, M. G.; Mihóková, E.; Martinez Turtos, R.; Lecoq, P.; Auffray, E.; Nikl, M. On the Structure, Synthesis, and Characterization of Ultrafast Blue-Emitting $CsPbBr_3$ Nanoplatelets. *APL Mater.* **2019**, *7*, No. 011104.
(67) Linaburg, M. R.; McClure, E. T.; Majher, J. D.; Woodward, P. M. $Cs_{1-X}Rb_xPbCl_3$ and $Cs_{1-X}Rb_xPbBr_3$ Solid Solutions: Understanding Octahedral Tilting in Lead Halide Perovskites. *Chem. Mater.* **2017**, *29*, 3507−3514.
(68) Zhu, S.; Ye, J.; Zhao, Y.; Qiu, Y. Structural, Electronic, Stability, and Optical Properties of $CsPb_{1-x}Sn_xIBr_2$ Perovskites: A First-Principles Investigation. *J. Phys. Chem. C* **2019**, *123*, 20476−20487.
(69) Cottingham, P.; Brutchey, R. L. On the Crystal Structure of Colloidally Prepared $CsPbBr_3$ Quantum Dots. *Chem. Commun.* **2016**, *52*, 5246−5249.
(70) Atourki, L.; Vega, E.; Mollar, M.; Marí, B.; Kirou, H.; Bouabid, K.; Ihlal, A. Impact of iodide substitution on the physical properties and stability of cesium lead halide perovskite thin films $CsPbBr_{3-x}I_x$ ($0 \le x \le 1$). *J. Alloys Compd.* **2017**, *702*, 404−409.
(71) Sharma, S.; Weiden, N.; Weiss, A. Phase Diagrams of Quasibinary Systems of the Type: ABX_3— $A'BX_3$; ABX_3— $AB'X_3$, and ABX3— ABX'_3; X = Halogen. *Zeitschrift für Physikalische Chemie.* **1992**, 63−80.
(72) Tenailleau, C.; Aharon, S.; Cohen, B.-E.; Etgar, L. Cell Refinement of $CsPbBr_3$ Perovskite Nanoparticles and Thin Films. *Nanoscale Adv.* **2019**, *1*, 147−153.
(73) Eperon, G. E.; Paternò, G. M.; Sutton, R. J.; Zampetti, A.; Haghighirad, A. A.; Cacialli, F.; Snaith, H. J. Inorganic Caesium Lead Iodide Perovskite Solar Cells. *J. Mater. Chem. A* **2015**, *3*, 19688−19695.
(74) Marronnier, A.; Roma, G.; Boyer-Richard, S.; Pedesseau, L.; Jancu, J. M.; Bonnassieux, Y.; Katan, C.; Stoumpos, C. C.; Kanatzidis, M. G.; Even, J. Anharmonicity and Disorder in the Black Phases of Cesium Lead Iodide Used for Stable Inorganic Perovskite Solar Cells. *ACS Nano* **2018**, *12*, 3477−3486.
(75) Liao, J.-F.; Rao, H.-S.; Chen, B.-X.; Kuang, D.-B.; Su, C.-Y. Dimension engineering on cesium lead iodide for efficient and stable perovskite solar cells. *J. Mater. Chem. A* **2017**, *5*, 2066−2072.
(76) Yang, D.; Cao, M.; Zhong, Q.; Li, P.; Zhang, X.; Zhang, Q. All-Inorganic Cesium Lead Halide Perovskite Nanocrystals: Synthesis, Surface Engineering and Applications. *J. Mater. Chem. C* **2019**, *7*, 757−789.
(77) Li, Z.; Yang, M.; Park, J.-S.; Wei, S.-H.; Berry, J. J.; Zhu, K. Stabilizing Perovskite Structures by Tuning Tolerance Factor: Formation of Formamidinium and Cesium Lead Iodide Solid-State Alloys. *Chem. Mater.* **2016**, *28*, 284−292.
(78) Travis, W.; Glover, E. N. K.; Bronstein, H.; Scanlon, D. O.; Palgrave, R. G. On the Application of the Tolerance Factor to Inorganic and Hybrid Halide Perovskites: A Revised System. *Chem. Sci.* **2016**, *7*, 4548−4556.
(79) Yan, L.; Xue, Q.; Liu, M.; Zhu, Z.; Tian, J.; Li, Z.; Chen, Z.; Chen, Z.; Yan, H.; Yip, H.-L.; et al. Interface Engineering for All-Inorganic $CsPbI_2Br$ Perovskite Solar Cells with Efficiency over 14%. *Adv. Mater.* **2018**, DOI: 10.1002/adma.201802509.
(80) Liu, S.; Chen, G.; Huang, Y.; Lin, S.; Zhang, Y.; He, M.; Xiang, W.; Liang, X. Tunable Fluorescence and Optical Nonlinearities of All Inorganic Colloidal Cesium Lead Halide Perovskite Nanocrystals. *J. Alloys Compd.* **2017**, *724*, 889−896.
(81) Zhang, P.; Zhu, G.; Shi, Y.; Wang, Y.; Zhang, J.; Du, L.; Ding, D. Ultrafast Interfacial Charge Transfer of Cesium Lead Halide Perovskite Films $CsPbX_3$ (X = Cl, Br, I) with Different Halogen Mixing. *J. Phys. Chem. C* **2018**, *122*, 27148−27155.
(82) Kang, B.; Biswas, K. Exploring Polaronic, Excitonic Structures and Luminescence in $Cs_4PbBr_6/CsPbBr_3$. *J. Phys. Chem. Lett.* **2018**, *9*, 830−836.
(83) Mao, X.; Sun, L.; Wu, T.; Chu, T.; Deng, W.; Han, K. First-Principles Screening of All-Inorganic Lead-Free ABX_3 Perovskites. *J. Phys. Chem. C* **2018**, *122*, 7670−7675.
(84) Hassanien, A. S.; Akl, A. A. Influence of Composition on Optical and Dispersion Parameters of Thermally Evaporated Non-Crystalline $Cd_{50}S_{50-X}Se_X$ Thin Films. *J. Alloys Compd.* **2015**, *648*, 280−290.
(85) El Radaf, I. M.; Al-Zahrani, H. Y. S.; Hassanien, A. S. Novel Synthesis, Structural, Linear and Nonlinear Optical Properties of p-Type Kesterite Nanosized Cu_2MnGeS_4 Thin Films. *J. Mater. Sci.: Mater. Electron.* **2020**, *31*, 8336−8348.
(86) Yadav, A. A.; Barote, M. A.; Dongre, P. M.; Masumdar, E. U. Studies on Growth and Characterization of $CdS_{1-x}Se_x$ ($0.0 \le x \le 1.0$) Alloy Thin Films by Spray Pyrolysis. *J. Alloys Compd.* **2010**, 179−185.
(87) Kumawat, N. K.; Tripathi, M. N.; Waghmare, U.; Kabra, D. Structural, Optical, and Electronic Properties of Wide Bandgap Perovskites: Experimental and Theoretical Investigations. *J. Phys. Chem. A* **2016**, *120*, 3917−3923.
(88) Li, M.; Zhang, X.; Du, Y.; Yang, P. Colloidal $CsPbX_3$ (X = Br, I, Cl) NCs: Morphology Controlling, Composition Evolution, and Photoluminescence Shift. *J. Lumin.* **2017**, *190*, 397−402.
(89) Li, X.; Wu, Y.; Zhang, S.; Cai, B.; Gu, Y.; Song, J.; Zeng, H. $CsPbX_3$ Quantum Dots for Lighting and Displays: Roomerature Synthesis, Photoluminescence Superiorities, Underlying Origins and White Light-Emitting Diodes. *Adv. Funct. Mater.* **2016**, *26*, 2435−2445.
(90) Bi, C.; Wang, S.; Li, Q.; Kershaw, S. V.; Tian, J.; Rogach, A. L. Thermally Stable Copper(II)-Doped Cesium Lead Halide Perovskite Quantum Dots with Strong Blue Emission. *J. Phys. Chem. Lett.* **2019**, *10*, 943−952.
(91) Zhyrair, G.; Lenrik, M.; Karapet, A.; Valeri, H.; Eduard, A.; Khachatur, M. Determination of the Complete Set of Optical Parameters of Micron-Sized Polycrystalline $CH_3NH_3PbI_{3-x}Cl_x$ Films from the Oscillating Transmittance and Reflectance Spectra. *Mater. Res. Express* **2020**, *7*, No. 016408.
(92) Swanepoel, R. Determination of the Thickness and Optical Constants of Amorphous Silicon. *J. Phys. E: Sci. Instrum.* **1983**, *16*, 1214−1222.
(93) Neumann, H.; Hörig, W.; Reccius, E.; Möller, W.; Kühn, G. Temperature Dependence of the Fundamental Absorption Edge in $CuGaSe_2$. *Solid State Commun.* **1978**, *27*, 449−451.
(94) Hameed, T. A.; Wassel, A. R.; El Radaf, I. M. Investigating the Effect of Thickness on the Structural, Morphological, Optical and Electrical Properties of $AgBiSe_2$ Thin Films. *J. Alloys Compd.* **2019**, *805*, 1−11.
(95) Kato, M.; Fujiseki, T.; Miyadera, T.; Sugita, T.; Fujimoto, S.; Tamakoshi, M.; Chikamatsu, M.; Fujiwara, H. Universal Rules for Visible-Light Absorption in Hybrid Perovskite Materials. *J. Appl. Phys.* **2017**, *121*, 115501.
(96) Hutter, E. M.; Sutton, R. J.; Chandrashekar, S.; Abdi-Jalebi, M.; Stranks, S. D.; Snaith, H. J.; Savenije, T. J. Vapour-Deposited Cesium Lead Iodide Perovskites: Microsecond Charge Carrier Lifetimes and Enhanced Photovoltaic Performance. *ACS Energy Lett.* **2017**, *2*, 1901−1908.
(97) Zhao, D.; Yu, Y.; Wang, C.; Liao, W.; Shrestha, N.; Grice, C. R.; Cimaroli, A. J.; Guan, L.; Ellingson, R. J.; Zhu, K.; et al. Low-Bandgap Mixed Tin-Lead Iodide Perovskite Absorbers with Long Carrier

Lifetimes for All-Perovskite Tandem Solar Cells. *Nat. Energy* **2017**, *2*, 17018.
(98) Wu, L.; Chen, K.; Huang, W.; Lin, Z.; Zhao, J.; Jiang, X.; Ge, Y.; Zhang, F.; Xiao, Q.; Guo, Z.; et al. Perovskite $CsPbX_3$: A Promising Nonlinear Optical Material and Its Applications for Ambient All-Optical Switching with Enhanced Stability. *Adv. Opt. Mater.* **2018**, *6*, 1800400.
(99) Ilcheva, V.; Petkov, P.; Boev, V.; Petkova, T. Optical Properties of Thermally Evaporated $(As2Se_3)_{100-X}Ag_x$ Thin Films. *Phys. Procedia* **2013**, *44*, 67−74.
(100) Yang, Y.; Ostrowski, D. P.; France, R. M.; Zhu, K.; Van De Lagemaat, J.; Luther, J. M.; Beard, M. C. Observation of a Hot-Phonon Bottleneck in Lead-Iodide Perovskites. *Nat. Photonics* **2016**, *10*, 53−59.
(101) Saba, M.; Cadelano, M.; Marongiu, D.; Chen, F.; Sarritzu, V.; Sestu, N.; Figus, C.; Aresti, M.; Piras, R.; Geddo Lehmann, A.; et al. Correlated Electron-Hole Plasma in Organometal Perovskites. *Nat. Commun.* **2014**, *5*, 5049.
(102) Hill, R. Energy-Gap Variations in Semiconductor Alloys. *J. Phys. C: Solid State Phys.* **1974**, *7*, 521−526.
(103) Hill, R.; Richardson, D. The Variation of Energy Gap with Composition in ZnS-Te Alloys. *J. Phys. C: Solid State Phys.* **1973**, *6*, L115.
(104) Venugopal, R.; Lin, P. I.; Chen, Y. T. Photoluminescence and Raman Scattering from Catalytically Grown $Zn_xCd_{1-x}Se$ Alloy Nanowires. *J. Phys. Chem. B* **2006**, *110*, 11691−11696.
(105) Noh, J. H.; Im, S. H.; Heo, J. H.; Mandal, T. N.; Seok, S. I. Chemical Management for Colorful, Efficient, and Stable Inorganic−Organic Hybrid Nanostructured Solar Cells. *Nano Lett.* **2013**, *13*, 1764−1769.
(106) Sharma, T. K.; Jangir, R.; Porwal, S.; Kumar, R.; Ganguli, T.; Zorn, M.; Zeimer, U.; Bugge, F.; Weyers, M.; Oak, S. M. Compositional Dependence of the Bowing Parameter for Highly Strained InGaAs/GaAs Quantum Wells. *Phys. Rev. B: Condens. Matter Mater. Phys.* **2009**, *80*, 165403.
(107) Ravi, V. K.; Markad, G. B.; Nag, A. Band Edge Energies and Excitonic Transition Probabilities of Colloidal $CsPbX_3$ (X = Cl, Br, I) Perovskite Nanocrystals. *ACS Energy Lett.* **2016**, *1*, 665−671.
(108) He, M.; Ding, L.; Liu, S.; Shao, G.; Zhang, Z.; Liang, X.; Xiang, W. Superior Fluorescence and High Stability of B-Si-Zn Glasses Based on Mn-Doped $CsPbBr_xI_{3-x}$ Nanocrystals. *J. Alloys Compd.* **2019**, *780*, 318−325.
(109) Akkerman, Q. A.; D'Innocenzo, V.; Accornero, S.; Scarpellini, A.; Petrozza, A.; Prato, M.; Manna, L. Tuning the Optical Properties of Cesium Lead Halide Perovskite Nanocrystals by Anion Exchange Reactions. *J. Am. Chem. Soc.* **2015**, *137*, 10276−10281.
(110) Li, N.; Zhu, Z.; Li, J.; Jen, A. K.-Y.; Wang, L. Inorganic $CsPb_{1-x}Sn_xIBr_2$ for Efficient Wide-Bandgap Perovskite Solar Cells. *Adv. Energy Mater.* **2018**, 1800525.
(111) Yang, Z.; Rajagopal, A.; Jen, A. K.-Y. Ideal Bandgap Organic − Inorganic Hybrid Perovskite Solar Cells. *Adv. Mater.* **2017**, 1704418.
(112) Ledinsky, M.; Schönfeldová, T.; Holovský, J.; Aydin, E.; Hájková, Z.; Landová, L.; Neyková, N.; Fejfar, A.; De Wolf, S. Temperature Dependence of the Urbach Energy in Lead Iodide Perovskites. *J. Phys. Chem. Lett.* **2019**, *10*, 1368−1373.
(113) De Wolf, S.; Holovsky, J.; Moon, S.-J.; Löper, P.; Niesen, B.; Ledinsky, M.; Haug, F. J.; Yum, J.-H.; Ballif, C. Organometallic Halide Perovskites: Sharp Optical Absorption Edge and Its Relation to Photovoltaic Performance. *J. Phys. Chem. Lett.* **2014**, *5*, 1035−1039.
(114) Abd-Elrahman, M. I.; Abu-Sehly, A. A.; Bakier, Y. M.; Hafiz, M. M. Thickness and Optical Constants Calculation for Chalcogenide-Alkali Metal $Se_{80}Te_8(NaCl)_{12}$ Thin Film. *Spectrochim. Acta, Part A* **2017**, *184*, 243−248.
(115) Al-Asbahi, B. A.; Qaid, S. M. H.; Hezam, M.; Bedja, I.; Ghaithan, H. M.; Aldwayyan, A. S. Effect of Deposition Method on the Structural and Optical Properties of $CH_3NH_3PbI_3$ Perovskite Thin Films. *Opt. Mater.* **2020**, *103*, 109836.
(116) El Radaf, I. M.; Hameed, T. A.; El komy, G. M.; Dahy, T. M. Synthesis, Structural, Linear and Nonlinear Optical Properties of Chromium Doped SnO_2 Thin Films. *Ceram. Int.* **2019**, *45*, 3072−3080.
(117) Yahia, I. S.; El Radaf, I. M.; Salem, A. M.; Sakr, G. B. Chemically Deposited Ni-Doped CdS Nanostructured Thin Films: Optical Analysis and Current-Voltage Characteristics. *J. Alloys Compd.* **2019**, *776*, 1056−1062.
(118) El-Bana, M. S.; El Radaf, I. M.; Fouad, S. S.; Sakr, G. B. Structural and Optoelectrical Properties of Nanostructured $LiNiO_2$ thin Films Grown by Spray Pyrolysis Technique. *J. Alloys Compd.* **2017**, *705*, 333−339.
(119) El-Nahass, M. M.; Farag, A. A. M.; El-Metwally, M.; Abu-Samaha, F. S. H.; Elesh, E. Structural, Absorption and Dispersion Characteristics of Nanocrystalline Copper Tetraphenyl Porphyrin Thin Films. *Synth. Met.* **2014**, *195*, 110−116.
(120) Yahia, I. S.; Ganesh, V.; Shkir, M.; Alfaify, S.; Zahran, H. Y.; Algarni, H.; Abutalib, M. M.; Al-Ghamdi, A. A.; El-Naggar, A. M.; Albassam, A. M. An Investigation on Linear and Non-Linear Optical Constants of Nano-Spherical CuPc Thin Films for Optoelectronic Applications. *Phys. B* **2016**, *496*, 9−14.

https://dx.doi.org/10.1021/acs.jpcc.0c07983
J. Phys. Chem. C 2021, 125, 886−897